



# Optical and ammonia sensing properties of Mn doped ZnO nanostructured films for gas sensors application

Sandhya Anil Jadhav<sup>1</sup> · M. B. Awale<sup>1</sup> · S. D. Lokhande<sup>1</sup> · G. Umadevi<sup>2</sup> · N. D. Raskar<sup>4</sup> · M. Vasundhara<sup>3</sup> · B. N. Dole<sup>4</sup> · Vishwanath D. Mote<sup>1</sup>

Received: 15 April 2024 / Accepted: 13 June 2024  
© Qatar University and Springer Nature Switzerland AG 2024

## Abstract

Mn-doped ZnO thin films were successfully developed via chemical spray pyrolysis technique and characterized using Field emission scanning electron microscopy (FESEM), Energy dispersive X-ray spectroscopy (EDAX), X-ray diffraction (XRD), UV–Vis Spectroscopy. An erected nanoplates-like morphology of Mn-doped ZnO films was observed through FESEM images. XRD results clearly indicated hexagonal (wurtzite) crystal structures of the undoped and Mn-doped ZnO films. Lattice parameters and volume of unit cell values were found to increase with the increase of Mn doping concentration. The optical band gap decreased from 3.28 eV to 3.26, on increase in Mn<sup>2+</sup> concentration. The ammonia gas sensing properties of the sensors based on undoped and Mn-doped ZnO films with low detection limit (15 ppm) at room temperature were investigated. The ammonia responses increased with increasing Mn doping concentration. The maximum response of 65%, 70% and 90% was acquired for ZnO, 2% and 4% Mn doped ZnO films at room temperature respectively. The ammonia sensor based on 4% Mn-doped ZnO nanostructures exhibited excellent sensing performance of ammonia concentration (15 ppm). The response and recovery times of 4% Mn-doped ZnO sensor towards 15 ppm NH<sub>3</sub> are 13 s and 7 s respectively. Gas sensing results bring promise to low operating temperature, low-cost NH<sub>3</sub> sensor based on Mn-doped ZnO, which could possibly used as real-time monitoring.

**Keywords** Mn doped ZnO thin films · X-ray diffraction · Optical properties · Erected nanoplates · Ammonia sensor

## 1 Introduction

Recently, fast advances in science and technology have resulted in significant changes in our day-to-day lives. During these developments, myriad environmental problems are

responsible for global concern. Particularly, environmental pollution affects not only ecosystem but also causes tremendous convulsions in living beings. Respiratory issues like asthma, suffocation and the cardiac problems in humans are increasing due to air pollution [1]. Hence, it has become mandatory to notice and control the hazardous gases in the environment. Last few years ago, various gas sensors are being fabricated and employed in diverse field of applications such as environmental analysis, breath sensors, automotive industry, indoor and outdoor air quality controls etc. However, there is a tremendous need for monitoring toxic gases including CO, CO<sub>2</sub>, NO, NO<sub>2</sub>, SO<sub>2</sub>, SO<sub>3</sub> and NH<sub>3</sub>. Among the innumerable gases, ammonia gas is commonly released from the various industries into the environment considered highly toxic, corrosive and causes danger to human life [2]. In addition, dairy and ice cream plants, wineries and breweries, petrochemical facilities, fruit juice, vegetable juice and soft drink processing facilities use huge amounts of ammonia as coolant. The higher concentrations of ammonia breathing can be hazardous to the lungs leading

✉ Vishwanath D. Mote  
vmote.physics@gmail.com

<sup>1</sup> Thin Films and Materials Science Research Laboratory, Department of Physics, Dayanand Science College, Latur 413512, Maharashtra, India

<sup>2</sup> Nanosensor Research Laboratory, Department of Physics, CMR Technical Campus, Medchal, Hyderabad 501-401, Telangana, India

<sup>3</sup> Polymer and Functional Department, CSIR-Indian Institute of Chemical Technology, Tarnaka, Hyderabad 500007, Telangana, India

<sup>4</sup> Advanced Materials Research Laboratory, Department of Physics, Dr. Babasaheb Ambedkar, Marathwada University, Sambhajinagar 431004, Maharashtra, India

to abnormalities related to respiration. Inhalation of ammonia gas for longer periods of time was one of the causes of people becoming more receptive to diseases like COVID-19 [3]. According to the survey of the Occupational Safety and Health Administration (OSHA), United States, the tolerable quantity of ammonia gas exposure edge to the humankind is on an average of 25 ppm for 8 h duration of a working day and 35 ppm for some time of 15 min. [4]. Hence, given this, there is an urge to develop efficient  $\text{NH}_3$  gas sensors, which can perform at minimum working temperature and can sense even low concentrations.

Recently, several methods are used to fabricate gas sensors for sensing ammonia which include conducting polymers [5], metal–organic frameworks [6], organic conjugated polymer [7], two-dimensional nanostructured materials [8] and metal oxide semiconductors [9]. Among the advanced sensing technologies, metal oxide semiconductors (such as CuO, ZnO, CoO,  $\text{SnO}_2$ ,  $\text{WO}_3$  etc.) system based sensors have been demonstrated good sensitivity, stability and selectivity to a particular gas [10]. Metal oxide semiconductors are readily available at low cost which work on the concept of variation in resistance in the presence of the analyte gases [9]. Metal oxide semiconductors due to their excellent property of gas detection are used to trace the gases like  $\text{O}_2$ ,  $\text{N}_2\text{O}$ ,  $\text{Cl}_2$ ,  $\text{NH}_3$ ,  $\text{H}_2$ , CO,  $\text{CH}_4$ , etc. [11]. Particularly, the n-type semiconducting metal oxides also have grabbed the attention of the researchers owing to their high selectivity, stability, and sensitivity towards the various oxidizing and reducing gases. The 2D transition metal dichalcogenides like  $\text{WS}_2$ ,  $\text{MoS}_2$ ,  $\text{WS}_2$ ,  $\text{MoSe}_2$ , etc. are also employed for room temperature sensing, improved selectivity, and performance. The major hindrance of these TMD's are slow recovery, the performance of which can be uplifted by UV illumination/thermal assistance yet an issue of power consumption arises [12]. Hence according to the review, the metal oxides/graphene-reduced metal oxides are used in the gas sensors in a wide range due to their high selectivity, quicker response, and recovery [13].

ZnO is one of the most important n-type metal oxide semiconductors with a relatively wide band gap and excellent chemical stability and has been investigated for its chemiresistive gas sensing [14]. In addition to these, it is also possesses other impressive properties likewise high thermal and chemical stability, catalytic activity, piezoelectric behavior, larger optical transparency in the visible region, low price, non-toxicity [15]. The development of ZnO thin films possessing the various surface morphologies like nanoplates, nanoflowers, nanotubes, nanorods, nanowires and so on has greatly expanded the specific surface area making which is suitable for widespread applications in different fields [16]. Nanostructures such as nanorods or nanowires have been proven to be better for gas sensing rather than nanoparticles, as they can boost the

substantiality of gas sensing [17]. Nevertheless, the semiconductor gas sensors usually work at high temperatures leading to high power consumption indirectly affecting their long-term stability and sensitivity [18]. This inflated temperature may also cause damage to the microstructure of the surface of the sensing material hence hampering its working capability and stability [4]. To recover this issue and enhance the gas sensitivity, the base material is doped with noble metals such as Au, Ag, Pt, etc. and transition metals like Co, Fe, Mn, Cu and Ni [19]. It has also been reported that the transition metal dopants like Mn, Al and so on are the rapid diffusing impurities in the conglomerated semiconductors [20].

M. Kumar and colleagues reported that the pure and Al-doped ZnO nanostructure films were highly selective and responsive towards CO gas due to surface defects of the sensors [21]. K. Ravichandran et al. studied the ZnO nanostructures were found to have highly appreciable for gas sensing activity [22]. Penga and group investigated the response of Mn-doped ZnO nanostructures towards the relative humidity at room temperature and earned better outcomes [23]. K. K. Khun et al., achieved better results for antimony-doped  $\text{SnO}_2$  thick films for detecting low concentrations of ammonia at room temperature [24]. Yuzhen Mao et al. studied the acetone sensing characteristics of Mn-doped ZnO samples and found satisfactory values of recovery and response time at an operating temperature of 340 °C [25]. Ahmed et al. investigated the Mn doping to ZnO nanorods to study the  $\text{O}_2$  sensing quality and obtained appreciable results at room temperature [26]. Henceforth, after going through the highlights of the above-mentioned studies, it is realized that ZnO samples doped with other metals and also doped with Mn are capable of sensing various gases like  $\text{O}_2$ , acetone, ethanol, humidity sensing, CO, and so on. As comparatively there is less work done on ammonia sensing characteristics and hence we decided to work on Mn-doped ZnO nanostructures.

At present, ZnO thin films are synthesized using numerous methods such as laser ablation, vapor deposition, sputtering, spray pyrolysis, CVD, sol–gel, CBD, etc. [27]. Of these, the spray pyrolysis method is a very accessible, inexpensive, secure, and capable of stoichiometry control and non-vacuum glazing method for synthesizing translucent and clear conducting oxides correlated with other methods [28].

Herein, we focus our attention on the development of pure and Mn doped ZnO gas sensors via spray pyrolysis. As per our literature analysis, no reports are available on sensing properties of Mn-doped ZnO towards ammonia for low concentration at room temperature. The main aim of this proposed work is to develop ZnO based thin films and to investigate their structural, optical, morphological, micro elemental, absorption, band gap and ammonia gas sensing performance at room temperature. Interestingly, the

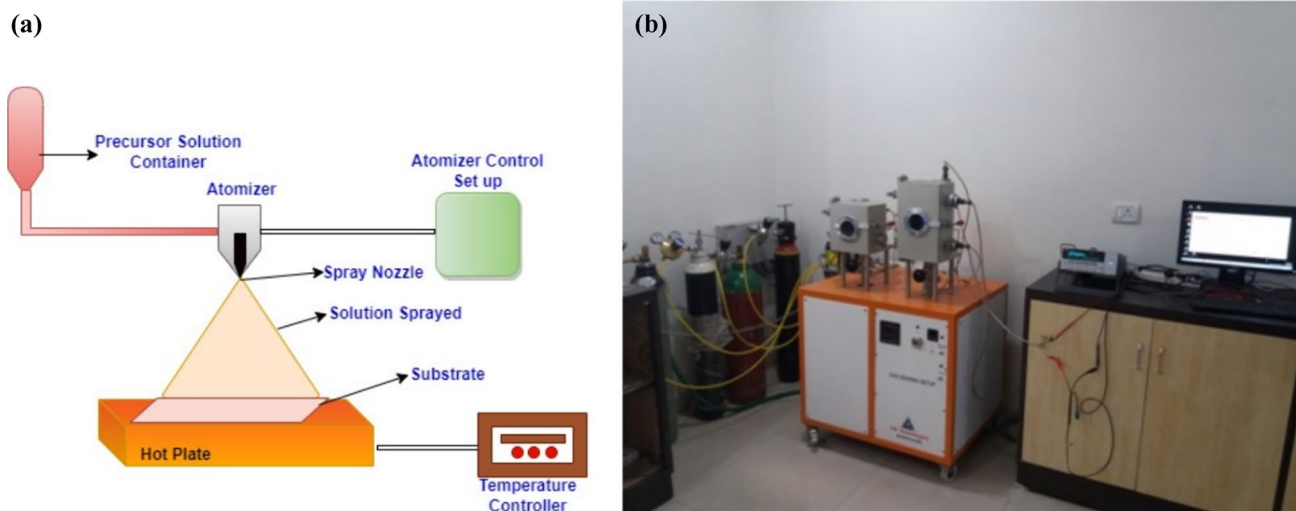


**Fig. 1** a Schematic diagram of spray pyrolysis setup; b Gas sensing apparatus arrangement

Mn-doped ZnO based sensors were more selective to ammonia and exhibiting high selectivity at room temperature.

## 2 Experimental section

### 2.1 Materials and methods

The preparation of high purity ZnO and Mn doped ZnO thin films were developed using commercial reagents. Zinc acetate dehydrate [ $\text{Zn}(\text{CH}_3\text{COO})_2 \cdot 2\text{H}_2\text{O}$ , 98%] as a precursor for zinc, manganese (II) acetate tetrahydrate [ $(\text{CH}_3\text{COO})_2\text{Mn} \cdot 4\text{H}_2\text{O}$ , 99%] as a dopant precursor were purchased from SIGMA-ALDRICH, distilled water used as oxidant.

### 2.2 Deposition of pure and Mn-doped ZnO thin films

Spray pyrolysis is a technique (a shown in Fig. 1(a)) based on droplet generation phenomenon with simple apparatus having striking properties like cost effectivity, simplicity, continuous operation, deposition on broad surfaces and higher rates of deposition. It is a flexible deposition technique for synthesizing single and multilayered films, dense or porous, ceramic coatings and so on. Deposition is undergone under the controlled parameters like substrate temperature, nozzle to substrate distance, pressure, spray rate, concentration of precursor solution etc.,

The foregoer materials zinc acetate dehydrate and manganese II acetate tetrahydrate were standardized according to the stoichiometric ratios to synthesize the pristine and Mn doped ZnO thin films. Zinc acetate was dissolved in a proper amount of double distilled water for making it a

0.1 M solution. The solution was stirred homogeneously at room temperature for 30 min, assigning a magnetic stirrer. Mn doping concentrations were followed to be 0, 2% and 4% respectively. Glass substrates were chosen for the deposition purpose. Before deposition the glass substrates were cleaned in the chromic acid and double distilled water and finally with acetone to remove all the contaminants. Initially, the air compressor of the spray pyrolysis unit was filled in order to avoid the pressure instability during the deposition. The sterilized glass substrates were pre-heated at a temperature  $400^\circ\text{C}$  by placing them on the metallic hot plate provided with the temperature controller. The solutions prepared were sprayed on the glass substrates with the help of atomizer at a spray rate of 2 ml/min. and maintaining nozzle to substrate distance at 20 cm and pressure at 30 psi. In like manner, Mn doped ZnO thin films were also deposited with changing Mn contents. The schematic processor of spray pyrolysis as shown in Fig. 1(a).

### 2.3 Characterization techniques

X-ray diffraction studies of the samples were conducted using RigakuUltima IV multifunctional X-Ray diffractometer (XRD) equipped with  $\text{CuK}\alpha 1$  source with wavelength  $1.5406 \text{ \AA}$ . The data range was obtained between  $10^\circ$  to  $90^\circ$ . Field emission scanning electron microscopy (FESEM) was performed by using NovaNanoSEM 308 for all the thin films. The energy dispersive X-ray spectroscopy (EDAX) was carried out to study the composition of the synthesized samples using Pegasus EDS-EBSD, JASCO-7310. Optical characterization of the deposited thin film samples was done using UV-Visible Spectrophotometer. The gas sensing performance of the deposited samples was studied

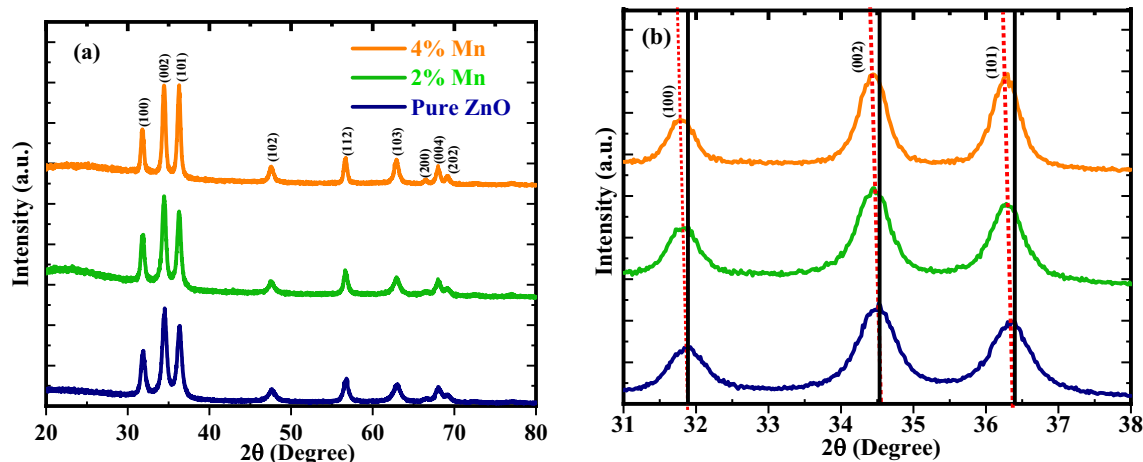


**Fig. 2** **a** Full angle range of XRD patterns and **b** high-resolution of (100) (002) (101) peak of the pure, 2 at%, and 4 at% Mn-doped ZnO samples

using Keithley electrometer (6517B) for various ammonia concentrations.

## 2.4 Fabrication of gas sensors

Figure 1(b) shows the gas sensing arrangement for measuring sensing property of the gas sensor. It comprises of an air tight (impenetrable) gas chamber specifically designed with inlet and outlet ports for letting the gas vapors inside and outside. This is mutually attached to a computer system and a high resistance Keithley source electrometer (6517B). The films at their edges of the substrate are scrapped off up to 2 mm and silver paste subsequently dispersed in ethyl alcohol is applied to establish electrical contacts upon the samples. These films are sintered at 100°C for 2 h in muffle furnace. Then the sensor to be tested for ammonia gas sensing is carefully placed inside the airtight chamber and then applied with a 4 V constant power supply across the samples to measure the fluctuations in resistance. The airtight chamber also dwells with a cylindrical flask used to fill the liquid gases to be tested. The vapors of these gases are produced by heating the flask at sufficient temperatures. Firstly, the chamber is kept open to measure the atmospheric air resistance so that a substantial baseline is attained. As soon as the substantial state is obtained, the heater is put on to produce the vapors of the liquid testing gases (here liquid ammonia is used) inside the cylindrical flask and the air-tight chamber is closed. The variation in the resistance concerning the substantial line was detected as a response to the testing gas vapors. These resistance fluctuations are noted from time to time.

The gas sensing measurements were performed in a 1 L stainless-steel chamber connected with a two-terminal source meter (Agilent B2902A) using a static volumetric method. The calculated volume of the target gas liquid was

injected using the following formula: Gas concentration (C) in parts per million (ppm) was determined using the static liquid gas distribution method. This calculation followed the formula:

$$C \text{ (ppm)} = \frac{22.4 \times V_1 \times D \times \varphi}{V_2 \times M} \quad (1)$$

Here D represents density (g/mL),  $\varphi$  is the required gas volume fraction,  $V_1$  and  $V_2$  represent the volume of the liquid and the chamber volume is measured in litres (L). M corresponds to the molecular weight of the liquid, expressed in grams per mole (g/mol) [29]. The sensitivity towards ammonia gas is evaluated using the relation [30]:

$$S(\%) = \frac{R_a - R_g}{R_a} \times 100 \quad (2)$$

where  $R_a$  and  $R_g$  are the resistances of the samples in the presence of air and analyte gas respectively.

## 3 Results and discussion

### 3.1 Structural studies

The phases and crystal structure of the developed films were investigated by XRD analysis. Figure 2(a) shows the XRD patterns for pristine ZnO and Mn-doped ZnO thin films. The observed diffraction peaks correspond to (100), (002), (101), (102), (110), (103), (112) for prepared films. The diffraction peaks of pure ZnO film were well indexed with hexagonal (wurtzite) phase of ZnO, indicating the successful formation of ZnO (JCPDS data card number 79-0206). The intensified diffraction peaks illustrate that the thin film samples have been highly crystalline in nature. No any additional Mn

**Table 1** XRD structural parameters of pure and Mn doped ZnO thin films

Samples	Crystallite size (nm)	Lattice Parameters		c/a ratio	Volume (Å) <sup>3</sup>	Bond length (Å)	Strain × 10 <sup>-3</sup>	Stress (GPa)	Dislocation density (δ) × 10 <sup>14</sup> m <sup>-2</sup>
		a (Å)	c (Å)						
Pure ZnO	13.13	3.2407	5.1952	1.6031	47.2527	1.9726	-1.69	0.393	58.00
2% Mn	14.20	3.2448	5.2035	1.6036	47.4464	1.9753	-0.096	0.022	49.59
4% Mn	18.68	3.2466	5.2042	1.6029	47.5054	1.9761	0.038	-0.008	28.65

phases were seen in Fig. 2(a) indicating the purity and the complex incorporation of the dopants into the ZnO samples which was also noted by Lekouiet. al. [31]. Ahmad et al. have reported to have additional impurity peaks are identified in the X-ray diffractograms due to the decomposition of MnO<sub>2</sub> into its lower oxides at elevated temperatures [32]. The dominant orientation being along (002) plane hints that the crystallites elected their preferred orientation along it. The heightened (101) peaks was also reported by Elavarasan and co-workers [33]. The similar results were also reported by Kicir and colleagues but along with this the (103) peak intensity which was increased initially and then decreased with Mn doping [34]. In addition, Fig. 2(b) shows the shift of (100), (002) and (101) peaks of Mn doped ZnO towards the lower angle side as compared to the pristine ZnO peaks with doping Mn content. In addition, significant changes in XRD peaks intensity were observed for Mn doped samples. From Fig. 2(b), it is also clear that the diffracted peaks broadening decreases with increasing Mn concentration. It indicates that high crystallinity with polycrystalline nature for doped films. This deviation of the peaks is illustrated in the following fashion: the concentration of the Mn impurity decreases from the surface to the core of the ZnO nanoplates and also towards the roots of the dispersed specimen [35]. Again, being the ionic radius of Mn<sup>2+</sup> slightly greater than the Zn<sup>2+</sup>, makes this shift towards the lower angle side. This peak shift mostly stresses on successful inclusion and uniform distribution of Mn<sup>2+</sup> ions into the ZnO lattice [36]. The crystallite size of the prepared thin films was calculated by applying the Debye–Scherrer’s formula which is given by [33]:

$$D = \frac{k\lambda}{\beta \cos\theta} \quad (3)$$

where k is the scherrer constant whose value is 0.9, λ is the wavelength of the CuKα source and is 1.5406 Å, full-width at half maxima (FWHM) is given by β, θ is the Bragg’s angle. The average crystallite size also enlarged from 13.13 nm to 18.24 nm for pure ZnO to 4% Mn-doped ZnO films (as tabulated in Table 1). The enhancement in average crystalline size owing to smaller grain growth of Mn doped ZnO as compared to pure ZnO films. The same type enhanced

crystallite has been reported by M. Harque and co-authors in their study on Mn doped ZnO nanopowder for ascertaining myocardial infarction through an electrochemical detection of myoglobin [37].

Lattice parameters were calculated using the following equation [38]:

$$\frac{1}{d^2} = \frac{4(h^2 + k^2 + l^2)}{3a^2} + \frac{l^2}{c^2} \quad (4)$$

where d<sub>hkl</sub> represents interplanar spacing, h, k and l are the miller indices. The lattice parameters a and c were observed to be increases with Mn content as tabulated in Table 1. This is pertaining to the ionic radius of Zn<sup>2+</sup> (0.74 Å) being smaller than that of Mn<sup>2+</sup> (0.80 Å). This can be elucidated by Vegard’s law according to which the discrepancy in the lattice parameters of the intrinsic and contaminated samples is due to their variation in the ionic radii of their respective ions [39]. Volume of the unit cell is determined using the equation [40]:

$$V = \frac{\sqrt{3}}{2} a^2 c \quad (5)$$

The volume of the unit cell of the pristine ZnO film as a function of Mn content as shown in Table 1. Analogous outcomes were by contemplated by Stefan et. al. [41]. This was attributed to the reinstatement of tetragonally coordinated larger Mn<sup>2+</sup> ions (0.80 Å) in place of smaller Zn<sup>2+</sup> ions (0.74 Å) which is associated with the induction of strains into the ZnO host matrix [41].

Further, the bond length of all the samples is calculated using the equation [38]:

$$L = \sqrt{\frac{a^2}{3} + \left(\frac{1}{2} - u\right)^2} \quad (6)$$

where u is known as the distortion parameter which is given by

$$u = \frac{a^2}{3c^2} + \frac{1}{4} \quad (7)$$

The bond length of Mn doped ZnO is found to be larger than that of pure ZnO which is shown in Table 1. Strain is



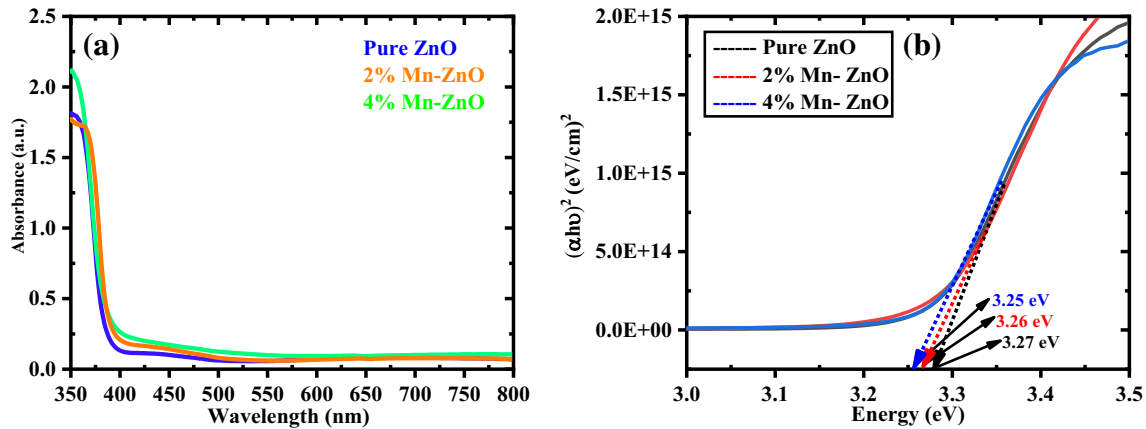


**Fig. 3** a UV–VIS Absorbance spectra of Undoped and Mn-doped ZnO thin films and bTauc's plot of the undoped and Mn-doped ZnO samples

generally created due to the disproportion in the substrate and the film. The strain ( $\epsilon$ ) and stress( $\sigma$ ) for the synthesized products can be found out by applying [39]:

$$\epsilon = (c_{\text{film}} - c_0)/c_0 \quad (8)$$

$$\sigma = -233 [(c_{\text{film}} - c_0)/c_0] \quad (9)$$

where  $c_{\text{film}}$  represents the calculated lattice parameter,  $c_0$  represents unstrained parameter whose value is given by  $c_0 = 5.204 \text{ \AA}$ . The negative values of strain indicate the compressive strain is raised due to doping and further doping led to the tensile strain. The values of strain are found to decrease with increasing Mn doping.

The length of the dislocation lines per unit volume of the crystal is the dislocation density ( $\delta$ ) which can be calculated by using equations [42]:

$$\delta = \frac{\frac{1}{D^2} \text{lines}}{\text{m}^2} \quad (10)$$

The dislocation density shrunk with the enhanced manganese content [43].

### 3.2 Optical analysis

Optical analysis of pure and Mn-doped ZnO films was carried out using UV–Vis spectrophotometer of model JASCO-7310 within the wavelength range of 350–800 nm as shown in Fig. 3. As the Mn doping content increases (as shown in Fig. 3(a)), absorption edge was found to be shifted towards the higher wavelength side which can be matched up with the variation of the optical bandgap which has also been proclaimed in earlier literature [44]. This improved absorbance in the visible region is interpreted as the enhancement of crystal defects present in the forbidden bandgap [45]. The

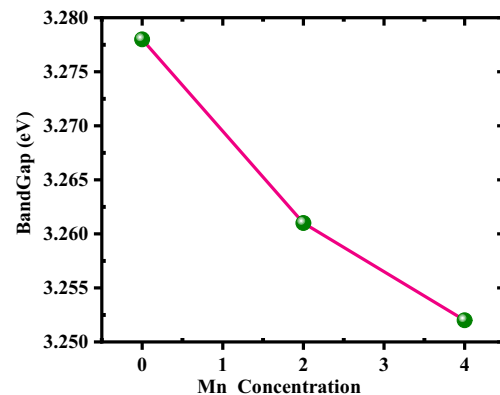


**Fig. 4** Band gap variation with doping concentration

relation between the absorption coefficient ( $\alpha$ ) and energy of the photon ( $h\nu$ ) is given by [46]:

$$\alpha h\nu = A(h\nu - E_g)^{1/2} \quad (11)$$

Figure 3(b). shows the plot of  $(\alpha h\nu)^2$  vs  $h\nu$ , from where the optical bandgap is evaluated for all the films. The optical bandgap values were observed to be decreased with increasing doping concentration of Mn as plotted in Fig. 4. The related work has been carried out by Strelchuk et al., and explained that the reduction in the bandgap as an account of exchange interactions between  $s$  and  $p$  electrons of ZnO matrix and  $d$  electrons of the dopant, which is explained using second-order perturbation theory [47]. Many other researchers also attributed this to the existence of crystal defects, like oxygen vacancies [48]. As noticed from the XRD results, the crystallite size is enhanced with the doping of Mn content. Here, we can observe a reverse relationship between the optical band gap and the crystallite size, which is adequate to conclude that the fabricated samples show the

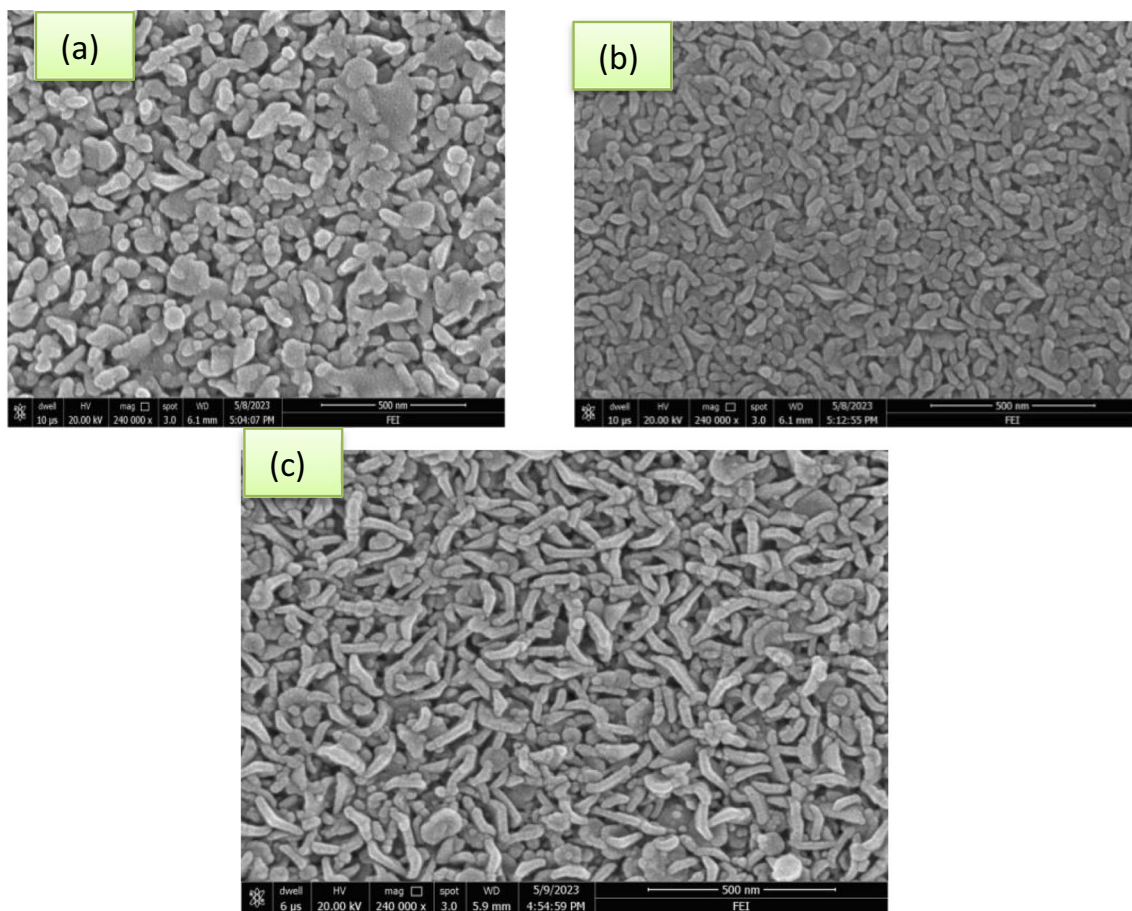


**Fig. 5** FESEM images of (a) Pure ZnO; (b) 2% Mn doped ZnO and (c) 4% Mn doped ZnO thin film

quantum confinement effect [49]. By looking at the above highlights, it is clear that the material is suitable for optoelectronic device applications.

### 3.3 Morphological analysis

Figure 5 (a-c) shows the FESEM micrograph images of pure ZnO, Mn doped ZnO thin film samples. FESEM micrograph of ZnO film showed the worm like morphology with fragmentary agglomerations as shown in Fig. 5(a). With enhanced Mn content, agglomerations were contemplated to be diminished leading to the increased worm size. 4% Mn doped ZnO sample attained morphology resembling nanoplates which were grown erect to the surface of the substrate. This was accompanied with prominent voids. The transformation of surface morphology from worm-like to vertical nanoplates is motivated mainly due to the successful incorporation of Mn into the ZnO lattice. The sharpened and elongated nanoplates depicts the enhanced crystallinity of the samples which can be correlated with the intensified (101) peak with Mn incorporation into the ZnO matrix which is shown in Fig. 2(a). The voids created in between the nanosheets are proved to be

advantageous for the sensitivity of gases which were analogously reported by N.Verma et. al., in their study of Sn doped ZnO nanostructures for sensor applications [50]. The morphological findings suggested that the voids are helpful for efficient gas sensing. The homologous morphologies were ascertained by H. Aledaghi et. al., in their research on the investigation of effects of growth parameters of ZnO nanostructures [51]. The synthesized vertical nanoplates being 1D ZnO nanostructures were proved to be highly profitable for gas sensor applications as their resistances are adjustable by the adsorbed gas species types onto their surfaces [52].

### 3.4 Compositional analysis

Figure 6 (a-c) reveals the elemental composition studies of the pure and Mn doped ZnO nanoplates undertaken through the Energy dispersive X-ray analysis. The intrinsic and Mn doped ZnO nanoplates are possessed with zinc, manganese and oxygen. The presence of Mn peak in Fig. 6(b) and (c) illustrates the appreciable addition of Mn into the ZnO matrix. Also EDAX spectrum shows no extra peaks indicating the purity of the synthesized Mn doped ZnO nanoplates.

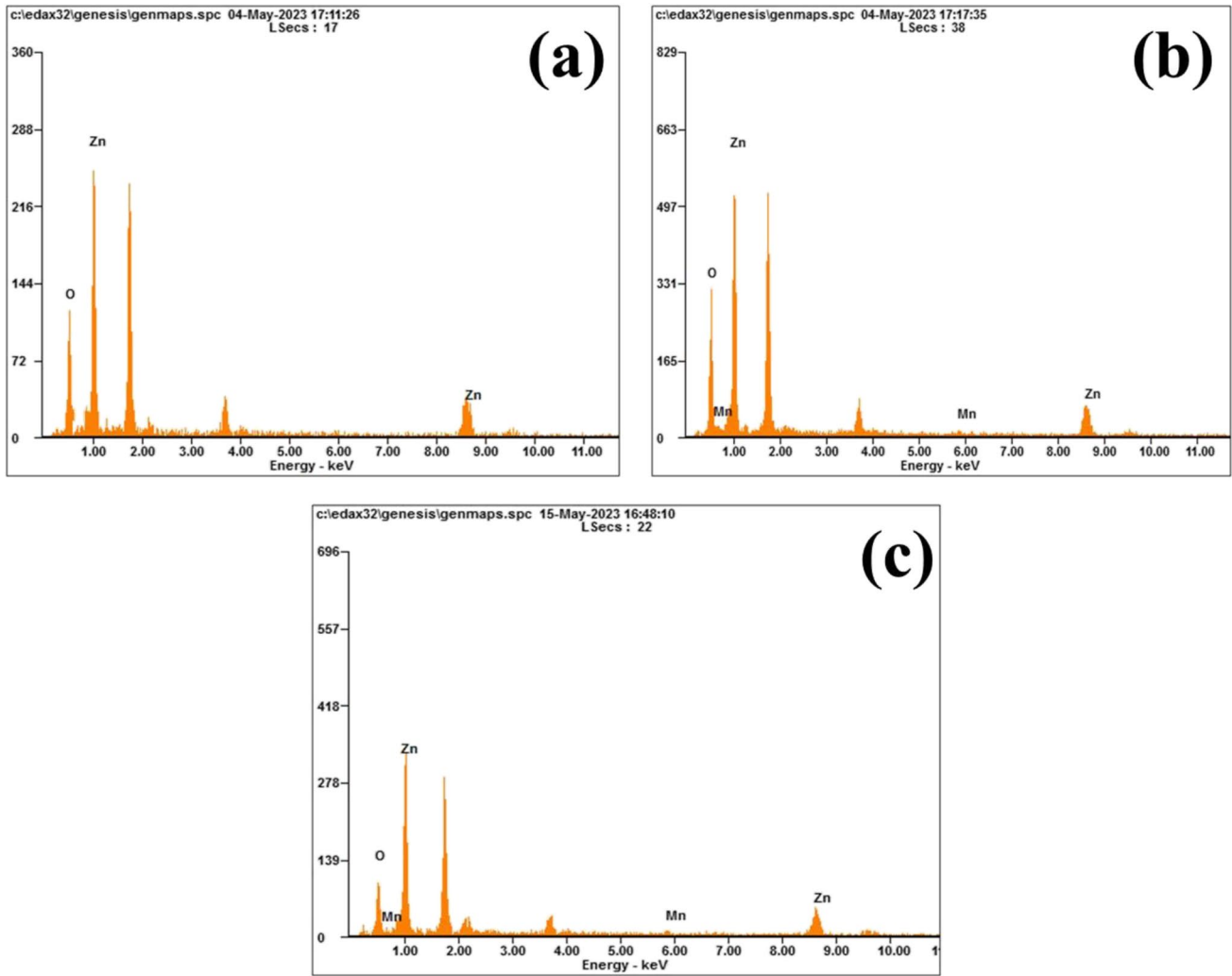


Fig. 6 EDAX Spectra of a) Pure ZnO b) 2% Mn doped ZnO and c) 4% Mn doped ZnO thin films

### 3.5 Gas sensing study

Gas sensing performance of the prepared pure and Mn doped ZnO films were carried out for different gases at room temperature. As shown in Fig. 7, the responses of the as developed films sensors to acetone, ethanol, xylene, ammonia and formaldehyde gases. It is confirmed a good selectivity towards to ammonia gas for developed films. If we compare the above results, we obtained a good sensitivity to ammonia gas over the other selected testing gases there fixed for 15 ppm level. From the above results, it emphasize that the prepared films have super sensitive and selective for ammonia gas sensing. Hence, we have chosen the ammonia gas for further studies.

Ammonia gas was used to demonstrate the room temperature gas sensing performance of the developed pure and Mn-doped ZnO thin films for 15 ppm. Figure 8 (a-c) shows the response of the ammonia sensor with undoped

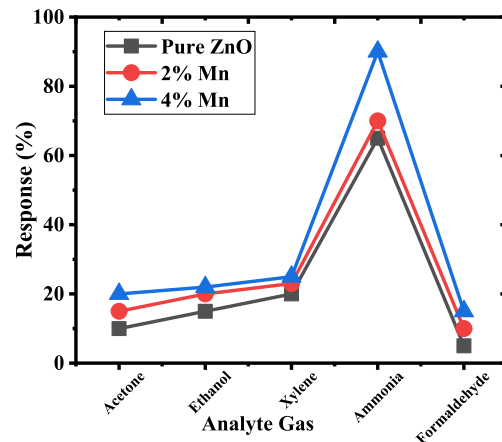
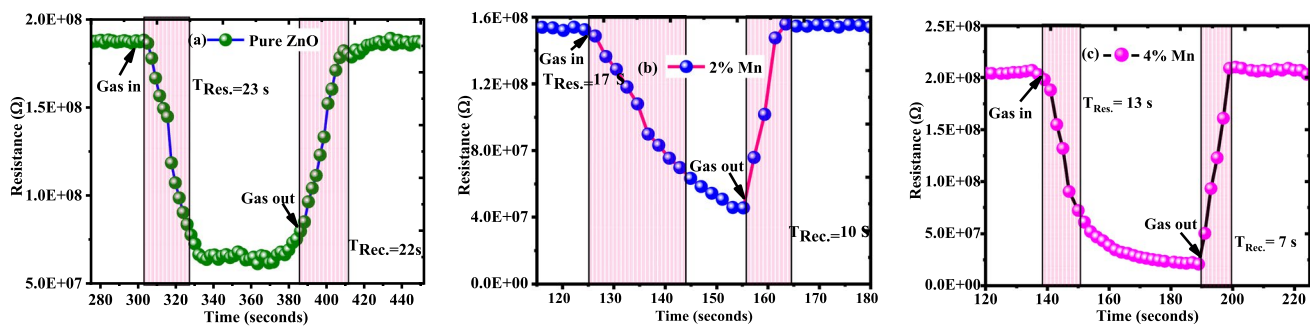


Fig. 7 Selectivity of pure, 2% and 4% Mn-doped ZnO thin films for different gases at 15 ppm concentration





**Fig. 8** Response and recovery times of (a) undoped, (b) 2% Mn doped and (c) 4% Mn doped ZnO samples

and Mn-doped ZnO films under 15 ppm ammonia at room temperature. The air resistance for pure ZnO and Mn doped ZnO films rapidly decreases when we introduce ammonia inside the chamber (as shown in Fig. 8). The air resistance sharply decreases because ammonia is a reducing gas and prepared films are n-type semiconductors. From Fig. 8 (c), it shows that 4% Mn-doped films exhibited higher sensing performance than that of the pristine ZnO film. The responses of films towards 15 ppm concentration are 65%, 70%, and 90% for 0%, 2%, and 4% Mn-doped correspondingly at room temperature. It emphasizes that 4% Mn-doped ZnO thin films exhibited superior ammonia gas sensing properties than the other prepared films. The response time and recovery time is calculated using the time versus resistance graph of the sensing factor of ammonia at 15 ppm. The calculated response and recovery times are given in Table 2. The response and recovery times for intrinsic ZnO thin film are found to be 23 s and 22 s respectively. With intensified doping content of Mn up to 2% and 4%, the response and recovery times took an edge off to 17 s and 10 s and 13 s, and 7 s respectively with stable baselines. The reduction in response time and recovery time in sensitivity attributes a higher Mn doping to the nanoplates and less agglomerations. Table 2 is epitomized in the form of a bar graph as shown in Fig. 9. It makes clear that the response recovery times decrease with Mn concentration.

Figure 10(a) shows the ammonia vapor response of the 4% Mn-doped ZnO film with varying ammonia concentration from 15 to 30 ppm. From Fig. 10(a), it is seen that as the concentration increases the sensitivity also value increase. This confirms that the quantity of vapor interacting with the

**Table 2** Recovery and Response times of Pure and Mn-doped ZnO samples

Samples	Response Time	Recover Time	Response
Pure ZnO	23 s	22 s	65%
2% Mn	17 s	10 s	70%
4% Mn	13 s	7 s	90%

surface of the Mn-doped ZnO films is a significant factor in determining the response. Also, the repeatability of all the samples was analyzed for the duration of 30 days to observe the response for 15 ppm ammonia gas concentration. The stable response was achieved for all the samples as shown in Fig. 10(b). Hence, the synthesized samples have a stable ammonia response at room temperature for 15 ppm concentration. Figure 10(c) shows gas response versus gas concentration plot which also shows a linear increase in response to increasing  $\text{NH}_3$  gas concentration. A response of 85.5% is obtained at 30 ppm for 4% Mn doped ZnO film.

This improved response of 4% Mn-doped ZnO thin film samples was attributed to the altered surface erected nanoplate morphology with innumerable voids which provided the proper gaps for the ammonia gas molecules to percolate onto the surface of the sample and also allows the trapped gas molecules to escape out, when the gas is sent out. Morphology in fact plays a very important role to shorten the response and recovery times. As the agglomerations decreased in the Mn contaminated samples in comparison to that of the pure sample which may be the one of the reasons for improved sensitivity. Sensitivity of any gas sensor is mainly related to the extent of diffusion of

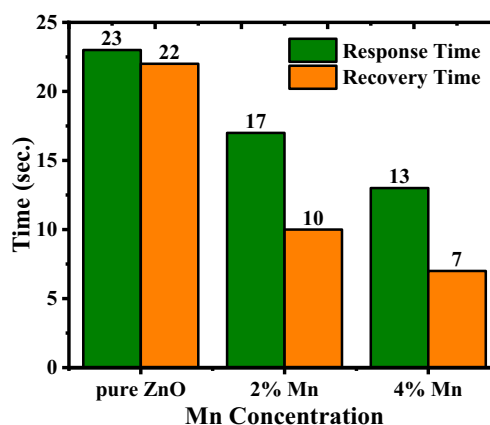


**Fig. 9** Response and recovery time Vs. Gas concentration with an error bar of undoped and Mn-doped ZnO films

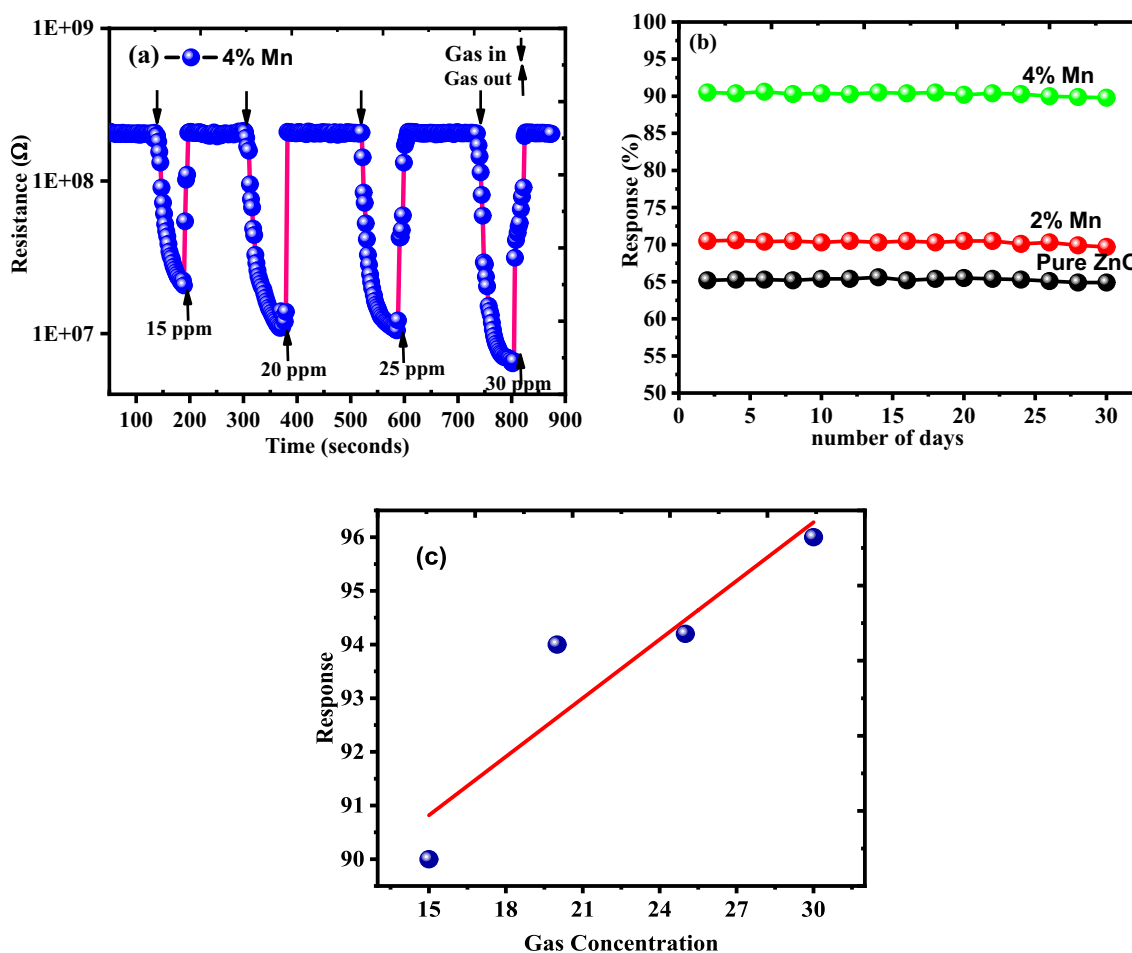


**Fig. 10** **a** Response-recovery curves of 4% Mn for different NH<sub>3</sub> gas concentrations; **b** repeatability of undoped, 2% Mn and 4% Mn-doped ZnO samples for 30 days to 15 ppm of NH<sub>3</sub> gas concentration; **c** sensor response vs NH<sub>3</sub> gas concentration

gas molecules of the specimen which is responsible to their absorption and desorption. But if there are more agglomerations on the film's surface, diffusion of gas molecules becomes more difficult into the agglomerated surface [53]. With the increased concentration level, enhanced sensitivity was observed which may be on the grounds that there will be an adequate amount of ammonia gas molecules available to interact with the surface of the specimen [54]. D. Wang et al., in their work studied that the Mn doped ZnO with hollow ball morphology were highly selective to the acetone gas [55]. R. S. Ganesh et al., achieved better response (28.5) for 8 wt% Mn doped ZnO nanospheres for 100 ppm but at 150 °C optimal temperature [56]. This was credited as an impact of Mn doping on pristine ZnO thin films. The sensitivity of 15.4% was ascertained for Mn doped ZnO thin films by T. Elavarasen et. al., in their research on Mn-doped ZnO nanostructures [57]. A. Ramesh and co-workers noted that Mn-doped ZnO nanospheres offered a response of 20.2 for 100 ppm ammonia gas concentration [58]. A more thorough literature survey has been displayed in the Table 3. Hence,

more clearly it confirms the worthy outcomes of the present work as compared to the above-mentioned literature, as the Mn doping to ZnO matrix presents the best response for 15 ppm ammonia concentration even at room temperature.

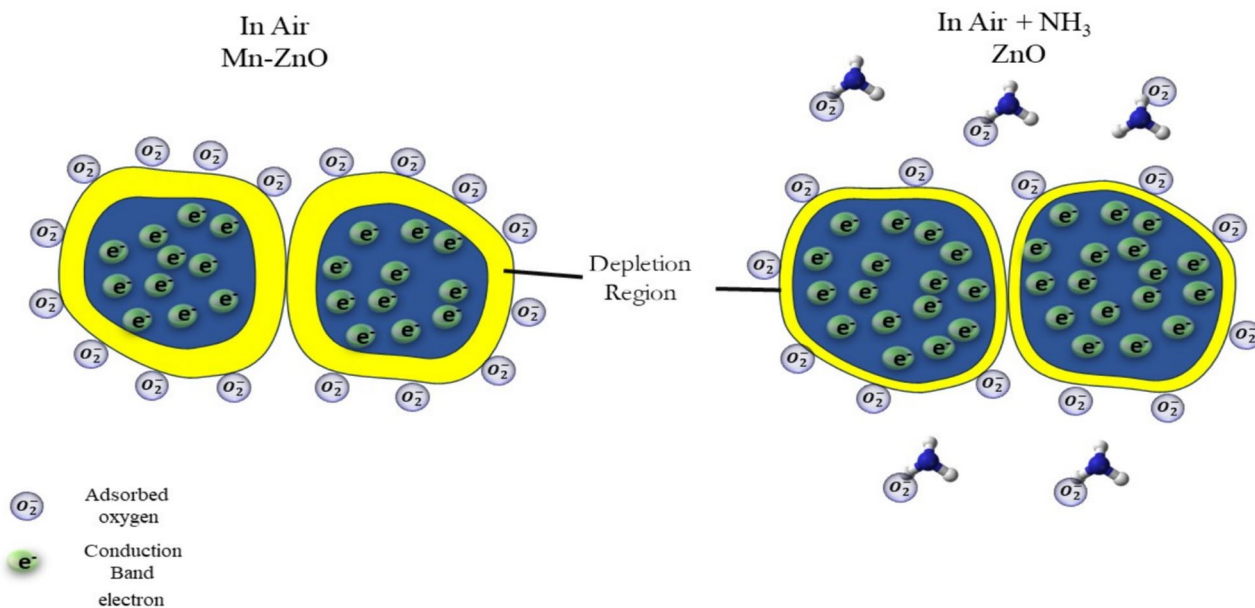
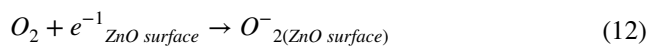
**Gas sensing mechanism** The technique of gas sensing is associated with the interaction of a gas and a solid at the surface of the thin film [19]. The interaction of the analytic gas molecules with surface varies the resistance of the semiconducting sample is the basic approach behind the gas sensing mechanism. This variation in resistance arises due the presence and absence of gas vapors. When the air-tight chamber is kept open, the atmospheric air interacts with the surface of the specimen. Hence, the oxygen molecules present in the air gets adsorbed on the surface of the film. Then the formation of oxygen ions takes place using the conduction band electrons of the ZnO thin film, which leads to the increase in thickness of the depletion layer, and thereby, increases the resistance of the film. It is because, when the ammonia gas comes in contact with the film surface, it reacts

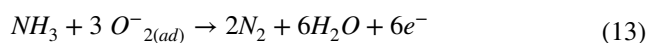
**Table 3** Review of Literature of various gas sensing samples

Sr.no	Metal doped ZnO gas sensor	Morphology	Analyte gas	Gas Concentration	Operating Temperature	Response time	Recovery time	Ref
1	ZnO	nanoparticles	O <sub>2</sub>	-	100° C	18	23	64
2	ZnO	nanocandles	CO	91	400 ° C	59	109	65
3	ZnO	Nanorods	NH <sub>3</sub>	10	300 ° C	193	98	66
4	Cd/ZnO	nanoparticles	ethanol	200	RT	125	-	67
5	Co/ZnO	Mixed shape nano-structures	TMA	50	100° C	19	15	68
6	Cu/ZnO	Spherical nano-structures	Acetaldehyde	100	100° C	16	18	69
7	Sn/ZnO	Spherical nano-structures	Acetone	100	100° C	30	63	70
8	Ag-ZnO/PANI	nanorods	NH <sub>3</sub>	120	RT	-	< 120	71
9	Ru/ZnO	Particles	NH <sub>3</sub>	1000	250 ° C	18	960	72
10	Al/ZnO	Nanosheet	NH <sub>3</sub>	50	100 ° C	29	19	73
11	Cu/ZnO	Nanoellipsoid	NH <sub>3</sub>	100	150 ° C	5.5	55	74
12	Ba doped ZnO	Agglomerated spherical grains	NH <sub>3</sub>	600	250°C	130	40	75
13	Mn doped ZnO	Hexagonal prismatic	NO <sub>2</sub>	10	75°C	107	158	76
14	Mn doped ZnO	Closely packed spherical grains	NH <sub>3</sub>	10 ppm	RT	49	170	77
15	Mn doped ZnO	Erected Nanoplates	NH <sub>3</sub>	15 ppm	RT	13	7	This work

with the adsorbed oxygen ions and the trapped electrons are released back into the conduction band, due to its reducing nature [59]. This leads to the decrease in the thickness of the depletion layer which in turn decreases the electrical

resistance followed by gain in conductivity [60]. This can be explained using the following reactions:

**Fig. 11** Gas sensing mechanism of Mn doped ZnO sample to the ammonia gas



The surface adsorbed oxygen molecules after trapping the electrons from the surface primarily forms three categories based on the operating temperature; 1.  $O_2^-$  ions are formed when the operating temperature is below  $100^\circ\text{C}$ , 2.  $O^-$  ions are formed when the operating temperature is in between  $100^\circ\text{C}$  to  $300^\circ\text{C}$  and 3.  $O^{2-}$  ions are formed when the operating temperature is above  $300^\circ\text{C}$  [61]. Hence, as mentioned in the referred literature, there is a possibility to form  $O_2^-$  ions in our fabricated Mn doped ZnO surface. Two factors are mainly responsible for an enhanced gas sensing nature of any sensor. One is the number of electrons trapped by the adsorbed oxygen atoms from the conduction band, and the second one is the number of electrons liberated back to the conduction band on encountering the sample surface with ammonia gas, which possesses reducing property [62]. Based on this, it is concluded that ammonia plays a crucial role in releasing the trapped electrons back into the conduction band from the adsorbed oxygen ions. This phenomenon is analyzed as the mechanism gas sensing for ammonia gas. According to the outcomes of our present study, more shortened response and recovery times were found than the pure ZnO samples. This is explained as in this sequential way. As observed from the FESEM micrographs we have discussed that the Mn enhanced ZnO samples had least agglomerations and also voids were also detected. These voids are considered to be the gaps or the defects formed on the surface of the samples which act as the oxygen adsorption centers to accommodate massive number of oxygen molecules from the atmospheric air. Hence, the Mn doping to the pure ZnO has developed more oxygen vacancies than the pure ZnO surface. So, when the highest Mn contented ZnO films is exposed to the atmospheric air placed in the gas sensing chamber, the enormous number of oxygen molecules get adsorbed on the surface and further gets ionized by trapping the electrons from the conduction band of the sample as shown in Fig. 11. This makes the depletion layer thicker and hence increasing resistance in the presence of the atmospheric air. Once the substantial baseline is reached, the ammonia gas vapors are introduced to the sample. Now this time, these enormous number of electrons get back into the conduction band making the depletion region more thinner and resistance decreases soon in a steeper line so as to record the least response and the recovery times as compared to the pristine ZnO. Based on this gas sensing studies, 4% Mn doped ZnO gas sensor is a promising material for ammonia gas sensing at low concentration (15 ppm) at room temperature.

## 4 Conclusion

In summary, ammonia sensor based on Mn-doped ZnO films has been developed by spray pyrolysis technique. The lattice parameters and volume of unit cell is found to have increased with the increase of Mn doping content. The optical absorption increases with increase in Mn concentration and the optical band gap values are witnessed to decrease from 3.27 eV to 3.25 eV, and Mn-doped ZnO films can be considered to have potential application in opto-electronics devices. The response time/recovery time values of pure ZnO, 2% and 4% Mn-doped ZnO films are found to have 23 s & 22 s, 17 s and 10 s, and 13 s and 7 s respectively. The 4% Mn doped ZnO thin films exhibited excellent ammonia vapor sensing properties with a high response of 90% in a low limit detection at room temperature owing to erected nanoplates like morphology with less agglomerations. Furthermore, the quick response/recovery time has endowed enhanced sensing performance as compared to undoped ZnO film. These results emphasize the potential application of prepared 4% Mn doped ZnO sensors for room temperature operating ammonia<sub>3</sub> gas sensor.

**Acknowledgements** The Author M. Vasundhara would like to acknowledge the support offered by Knowledge & Information Management CSIR-Indian Institute of Chemical Technology (IICT/Pubs./2024/210).

**Authors contribution** Sandhya A. Jadhav: Conceptualization, Investigation, Methodology, M. B. Awale: Formal analysis. S. D. Lokhande: Formal analysis. G. Umadevi: Data curation. N. D. Raskar: Formal M. Vasundhara: Writing – review & editing, B. N. Dole: Writing – review & editing, V. D. Mote: Writing – review & editing, Supervision, Resources.

**Data availability** Data sets generated during the current study are available from corresponding author on reasonable request.

## Declarations

**Competing interest** The authors declare that they have no known competing financial interests or personal relationships that could have appeared to influence the work reported in this paper.

## References

1. M.E. Manager, Human health and environmental impacts of coal combustion and post-combustion wastes. *J. Sustain. Min.* **1**, 87–96 (2017)
2. Xu, Liu, N. Chen, B. Han, X. Xiao, G. Chen, I. Djerdj, Y. Wang, Nanoparticle cluster gas sensor: Pt activated SnO<sub>2</sub> nanoparticles for NH<sub>3</sub> detection with ultrahigh sensitivity. *Nanoscale* **7**, 14872–14880 (2015)
3. X. Zeng, J. Li, B. Shen, Novel approach to recover cobalt and lithium from spent lithium-ion battery using oxalic acid. *J. Hazard. Mater.* **295**, 112–118 (2015)

4. J. Wen et al., MXene-derived TiO<sub>2</sub> nanosheets decorated with Ag nanoparticles for highly sensitive detection of ammonia at room temperature. *J. Mater. Sci. Technol.* **114**, 233–239 (2022)
5. F. Ranjbar, S. Hajati, M. Ghaedi, K. Dashtian, H. Naderi, J. Toth, Highly selective MXene/V<sub>2</sub>O<sub>5</sub>/CuWO<sub>4</sub>-based ultra-sensitive room temperature ammonia sensor. *J. Hazard. Mater.* **416**, 126196 (2021)
6. Z. Duan et al., Novel application of attapulgite on high performance and low-cost humidity sensors. *Sensors Actuators B Chem.* **305**, 127534 (2020)
7. M.-S. Song et al., Recent advances in biodegradation controls over Mg alloys for bone fracture management: A review. *J. Mater. Sci. Technol.* **35**, 535–544 (2019)
8. S.M. Majhi, A. Mirzaei, H.W. Kim, S.S. Kim, T.W. Kim, Recent advances in energy-saving chemiresistive gas sensors: A review. *Nano Energy* **79**, 105369 (2021)
9. Y.R. Kumar, K. Deshmukh, K.K. Sadasivuni, S.K.K. Pasha, Graphene quantum dot based materials for sensing, bio-imaging and energy storage applications: a review. *RSC Adv.* **10**, 23861–23898 (2020)
10. S. Benramache, A. Arif, O. Belahssen, A. Guettaf, Study on the Correlation between the crystallite size and optical band gap energy of doped ZnO thin films. *J. Nanostruct. Chem.* **3**, 1–6 (2013)
11. B. Saruhan, R. LontioFomekong, S. Nahirniak, Review: Influences of Semiconductor Metal Oxide Properties on Gas Sensing Characteristics. *Front. Sensors* **2**, 1–24 (2021)
12. S. Yang, C. Jiang, S. H. Wei, Gas sensing in 2D materials, *Appl. Phys. Rev.* **4**, 2 (2017). <https://doi.org/10.1063/1.4983310>
13. N. Joshi, T. Hayasaka, Y. Liu, H. Liu, O. N. Oliveira, and L. Lin, A review on chemiresistive room temperature gas sensors based on metal oxide nanostructures, graphene and 2D transition metal dichalcogenides, *Microchim. Acta* **185**, 4 (2018). <https://doi.org/10.1007/s00604-018-2750-5>
14. W. Majeed, Z. Imran, S. Hassan, M. Ahmad, and S. S. Batool, Low temperature dielectric study and photoconductive analysis of ZnO/NiO composite material, *Ceram. Int.*, **15**, 17736–17746 (2024)
15. M. Willander, M.Q. Israr, J.R. Sadaf, O. Nur, No Title. *Nanophotonics* **1**, 99–115 (2012)
16. P. Obreja, D. Cristea, A. Dinescu, C. Romanițan, Influence of surface substrates on the properties of ZnO nanowires synthesized by hydrothermal method. *Appl. Surf. Sci.* **463**, 1117–1123 (2019)
17. K.J. Choi, H.W. Jang, One-Dimensional Oxide Nanostructures as Gas-Sensing Materials: Review and Issues. *Sensors* **10**, 4083–4099 (2010)
18. S. Ranwa, P.K. Kuliya, V.K. Sahu, L.M. Kukreja, M. Kumar, Defect-free ZnO nanorods for low temperature hydrogen sensor applications. *AIP Publishing* **105**, 213103 (2014)
19. R.S. Ganesh et al., Tuning the selectivity of NH<sub>3</sub> gas sensing response using Cu-doped ZnO nanostructures. *Sensors Actuators A Phys.* **269**, 331–341 (2018)
20. A.J. Kulandaisamy, C. Karthek, P. Shankar, G.K. Mani, J.B.B. Rayappan, Tuning selectivity through cobalt doping in spray pyrolysis deposited ZnO thin films. *Ceram. Int.* **42**, 1408–1415 (2016)
21. M. Kumar et al., Effect of structural defects, surface roughness on sensing properties of Al doped ZnO thin films deposited by chemical spray pyrolysis technique. *Ceram. Int.* **43**, 3562–3568 (2017)
22. K. Ravichandran, A. Manivasaham, K. Subha, A. Chandrabose, R. Mariappan, Cost-effective nebulizer sprayed ZnO thin films for enhanced ammonia gas sensing – Effect of deposition temperature. *Surfaces Interfaces* **1–3**, 13–20 (2016)
23. X. Peng, J. Chu, B. Yang, P.X. Feng, Mn-doped zinc oxide nanopowders for humidity sensors. *Sensors Actuators B Chem.* **174**, 258–262 (2012)
24. K. KhunKhun, A. Mahajan, R.K. Bedi, Nanostructured Sb doped SnO<sub>2</sub> thick films for room temperature NH<sub>3</sub> sensing. *Chem. Phys. Lett.* **492**(1), 119–122 (2010). <https://doi.org/10.1016/j.cplett.2010.04.039>
25. Y. Mao et al., Effect of Mn doping on the microstructures and sensing properties of ZnO nanofibers. *Appl. Surf. Sci.* **298**, 109–115 (2014)
26. F. Ahmed, N. Arshi, M.S. Anwar, R. Danish, B.H. Koo, Mn-doped ZnO nanorod gas sensor for oxygen detection. *Curr. Appl. Phys.* **13**, S64–S68 (2013)
27. M. Gartner, H. Stroescu, D. Mitrea, M. Nicolescu, Various Applications of ZnO Thin Films Obtained by Chemical Routes in the Last Decade. *Molecules* **28**, 12 (2023)
28. M.M.A. Ahmed, W.Z. Tawfik, M.A.K. Elfayoumi, M. Abdel-Hafez, S.I. El-Dek, Tailoring the optical and physical properties of La doped ZnO nanostructured thin films. *J. Alloys Compd.* **791**, 586–592 (2019)
29. S. Sardana, H. Kaur, B. Arora, Dinesh Kumar Aswal, and Aman Mahajan. *ACS Sens.* **7**, 312–321 (2022)
30. S.P.S. David, S. Veeralakshmi, S. Nehru, S. Kalaiselvam, A highly sensitive, selective and room temperature operatable formaldehyde gas sensor using chemiresistive g-C<sub>3</sub>N<sub>4</sub>/ZnO. *Mater. Adv.* **1**, 2781–2788 (2020)
31. F. Lekoui et al., Investigation of the effects of thermal annealing on the structural, morphological and optical properties of nanostructured Mn doped ZnO thin films. *Opt. Mater. (Amst)* **118**, 111236 (2021)
32. S.A. Ahmed, Structural, optical, and magnetic properties of Mn-doped ZnO samples. *Results Phys.* **7**, 604–610 (2017)
33. A.J. Kulandaisamy et al., Room temperature ammonia sensing properties of ZnO thin films grown by spray pyrolysis: Effect of Mg doping. *J. Alloys Compd.* **688**, 422–429 (2016)
34. A.K. Ambedkar et al., Structural, optical and thermoelectric properties of Al-doped ZnO thin films prepared by spray pyrolysis. *Surfaces Interfaces* **19**, 100504 (2020)
35. J. Panda, I. Sasmal, T.K. Nath, Magnetic and optical properties of Mn doped ZnO vertically aligned nanorods, synthesized by hydrothermal technique. *AIP Adv.* **6**, 35118 (2016)
36. S. Balamurali, S. Saravanakumar, R. Chandramohan, P.N. Magudeswaran, SILAR Technique-Grown Mn-doped ZnO Thin Films. *Brazilian J. Phys.* **51**, 1501–1508 (2021)
37. M. Haque, H. Fouad, H.K. Seo, A.Y. Othman, A. Kulkarni, Z.A. Ansari, Investigation of Mn doped ZnO nanoparticles towards ascertaining myocardial infarction through an electrochemical detection of myoglobin. *IEEE Access* **8**(Cvd), 164678–164692 (2020)
38. A. Dhanalakshmi, S. Thanikaikarasan, B. Natarajan, Influence of Mn dopant concentration on film thickness, structural, morphological, compositional and optical properties of zinc oxide thin films. *J. Mater. Sci. Mater. Electron.* **28**, 11576–11583 (2017)
39. T.A. Abdel-Baset, M. Abdel-Hafez, Effect of metal dopant on structural and magnetic properties of ZnO nanoparticles. *J. Mater. Sci. Mater. Electron.* **32**, 16153–16165 (2021)
40. A. Salah, A.M. Saad, A.A. Aboud, Effect of Co-doping level on physical properties of ZnO thin films. *Opt. Mater. (Amst)* **113**, 110812 (2021)
41. T. Elavarasan, S. Ernest, S. Fairrose, Spray deposited nanostructured ZnO: Mn thin films for ammonia vapour sensing application. *Mater. Today Proc.* **38**, 2839–2844 (2020)
42. M. Stefan, D. Ghica, S.V. Nistor, A.V. Maraloiu, R. Plugaru, Mn<sup>2+</sup> ions distribution in doped sol–gel deposited ZnO films. *Appl. Surf. Sci.* **396**, 1880–1889 (2017). <https://doi.org/10.1016/j.apsusc.2016.02.167>



43. H.S. Sindhu, S.R. Maidur, P.S. Patil, R.J. Choudhary, B.V. Rajendra, Nonlinear optical and optical power limiting studies of Zn<sub>1-x</sub>MnxO thin films prepared by spray pyrolysis. *Optik (Stuttg)* **132**, 671–681 (2019)
44. Q. Ma, X. Lv, Y. Wang, J. Chen, Optical and photocatalytic properties of Mn doped flower-like ZnO hierarchical structures. *Opt. Mater. (Amst)* **60**, 86–93 (2016)
45. B. Sambandam, R.J.V. Michael, P.T. Manoharan, Oxygen vacancies and intense luminescence in manganese loaded ZnO microflowers for visible light water splitting. *Nanoscale* **7**, 13935–13942 (2015)
46. X.J. Liu, C. Song, F.F. Zeng, X.B. Wang, F. Pan, Influence of annealing on microstructure and magnetic properties of co-sputtered Co-doped ZnO thin films. *J. Phys. D Appl. Phys.* **40**, 1608–1613 (2007)
47. V.V. Strelchuk et al., Optical and structural properties of Mn-doped ZnO nanorods grown by aqueous chemical growth for spintronic applications. *Thin Solid Films* **601**, 22–27 (2016)
48. R. Ullah, J. Dutta, Photocatalytic degradation of organic dyes with manganese-doped ZnO nanoparticles. *J. Hazard. Mater.* **156**, 194–200 (2008)
49. M.E. Ghazi, M. Izadifard, F.E. Ghodsi, M. Yuonesi, Studying Mn and Ni-doped ZnO thin films synthesized by the Sol-gel method. *J. Supercond. Nov. Magn.* **25**, 101–108 (2012). <https://doi.org/10.1007/s10948-011-1213-6>
50. S. Bhatia, N. Verma, R.K. Bedi, Sn-doped ZnO nanopetal networks for efficient photocatalytic degradation of dye and gas sensing applications. *Appl. Surf. Sci.* **407**, 495–502 (2017)
51. H. Alehdaghi, M. Zirak, Facile preparation of various ZnO nanostructures via ultrasonic mist vapor deposition : a systematic investigation about the effects of growth parameters. *J. Mater. Sci. Mater. Electron* (2019). <https://doi.org/10.1007/s10854-018-0546-3>
52. N. Kicir, T. Tüken, M. Akyol, A. Ekcicibil, Y. Ufuktepe, Structural, electronic and magnetic properties of Mn doped ZnO nanoplates synthesized by electrodeposition method. *J. Electron Spectros. Relat. Phenomena* **237**, 146892 (2019)
53. M.R. Prasad, M. Haris, M. Sridharan, NH<sub>3</sub> sensing properties of surface modified Ce-doped nanostructured ZnO thin films prepared by spray pyrolysis method. *Sensors Actuators A Phys.* **269**, 435–443 (2018)
54. K. Ravichandran, A.J. Santhosam, M. Sridharan, Effect of tungsten doping on the ammonia vapour sensing ability of ZnO thin films prepared by a cost effective simplified spray technique. *Surfaces Interfaces* **18**, 100412 (2020). <https://doi.org/10.1016/j.surfin.2019.100412>
55. D. Wang, W. Shang, B. Zhang, C. Jiang, F. Qu, and M. Yang, Manganese-doped zinc oxide hollow balls for chemiresistive sensing of acetone vapors. *Microchim Acta* **186**, 44 (2019)
56. R. Sankar Ganesh et al., Low temperature ammonia gas sensor based on Mn-doped ZnO nanoparticle decorated microspheres. *J. Alloys Compd.* **721**, 182–190 (2017)
57. T. Elavarasan, S. Ernest, S. Fairose, Spray deposited nanostructured ZnO: Mn thin films for ammonia vapour sensing application. *Mater. Today Proc.* **38**, 2839–2844 (2021)
58. A. Ramesh, D.S. Gavaskar, P. Nagaraju, S. Duvvuri, S.R.K. Vanjari, C. Subrahmanyam, Mn-doped ZnO microspheres prepared by solution combustion synthesis for room temperature NH<sub>3</sub> sensing. *Appl. Surf. Sci. Adv.* **12**, 100349 (2022)
59. N.S. Ramgir et al., Room temperature H<sub>2</sub>S sensor based on Au modified ZnO nanowires. *Sensors Actuators B Chem.* **186**, 718–726 (2013)
60. K.D. Arun Kumar et al., Effect of Er doping on the ammonia sensing properties of ZnO thin films prepared by a nebulizer spray technique. *J. Phys. Chem. Solids* **144**, 109513 (2020)
61. K.D. Arun Kumar et al., Effect of Er doping on the ammonia sensing properties of ZnO thin films prepared by a nebulizer spray technique. *J. Phys. Chem. Solids* **144**, 109513 (2020). <https://doi.org/10.1016/j.jpcs.2020.109513>
62. N.S. Ramgir et al., Room temperature H<sub>2</sub>S sensor based on Au modified ZnO nanowires. *Sensors Actuators B Chem.* **186**, 718–726 (2013). <https://doi.org/10.1016/j.snb.2013.06.070>
63. M.Y. Al-darwesh, S.S. Ibrahim, M. FaiadNaief, A. Mishaal Mohammed, H. Chebbi, Synthesis and characterizations of zinc oxide nanoparticles and its ability to detect O<sub>2</sub> and NH<sub>3</sub> gases. *Results Chem.* **6**, 101064 (2023). <https://doi.org/10.1016/j.rechem.2023.101064>
64. R. Godiwal et al., Synthesis and growth mechanism of ZnO nanocandles using thermal evaporation and their efficient CO sensing performance. *Micro Nanostruct.* **184**, 207692 (2023). <https://doi.org/10.1016/j.micrna.2023.207692>
65. T.-Y. Chen et al., Characteristics of ZnO nanorods-based ammonia gas sensors with a cross-linked configuration. *Sensors Actuators B Chem.* **221**, 491–498 (2015). <https://doi.org/10.1016/j.snb.2015.06.122>
66. B. Singh et al., Synthesis of cadmium-doped zinc oxide nanoparticles via sol-gel method for ethanol gas sensing application. *J. Mater. Sci.: Mater. Electron.* **34**(13), 1114 (2023)
67. J. Rodrigues, N.G. Shimpi, Detection of trimethylamine (TMA) gas using mixed shape cobalt doped ZnO nanostructure. *Mater. Chem. Phys.* **305**, 127972 (2023). <https://doi.org/10.1016/j.matchemphys.2023.127972>
68. J. Rodrigues, V. Borge, S. Jain, N.G. Shimpi, Enhanced Acetaldehyde Sensing Performance of Spherical Shaped Copper Doped ZnO Nanostructures. *Chem. Eur.* **8**, e202203967 (2023)
69. J. Rodrigues, S. Jain, N.G. Shimpi, Performance of 1D tin (Sn) decorated spherical shape ZnO nanostructures as an acetone gas sensor for room and high temperature. *Mater. Sci. Eng. B* **288**, 116199 (2023). <https://doi.org/10.1016/j.mseb.2022.116199>
70. N. Karmakar, S. Jain, R. Fernandes, A. Shah, U. Patil, N. Shimpi, D. Kothari, Enhanced sensing performance of ammonia gas sensor Based on Ag decorated ZnO Nanorods/Polyaniline Nanocomposite. *Chem. Eur.* **8** (2023)
71. K.R. Devi et al., Enhanced room temperature ammonia gas sensing properties of Al-doped ZnO nanostructured thin films. *Opt. Quantum. Electron.* **52**(11), 1–19 (2020). <https://doi.org/10.1007/s11082-020-02621-0>
72. L.H. Kathwate et al., Ammonia gas sensing properties of Al doped ZnO thin films. *Sensors Actuators A Phys.* **313**, 112193 (2020). <https://doi.org/10.1016/j.sna.2020.112193>
73. R.S. Ganesh et al., Tuning the selectivity of NH<sub>3</sub> gas sensing response using Cu-doped ZnO nanostructures. *Sensors Actuators A Phys.* **269**, 331–341 (2018). <https://doi.org/10.1016/j.sna.2017.11.042>
74. V. Gopala Krishnan, P. Elango, Influence of Ba doping concentration on the physical properties and gas sensing performance of ZnO nanocrystalline films: Automated nebulizer spray pyrolysis (ANSP) method. *Optik (Stuttg)* **141**, 83–89 (2017). <https://doi.org/10.1016/j.ijleo.2017.05.045>
75. K. Suganthi, E. Vinoth, L. Sudha, P. Bharathi, M. Navaneethan, Manganese (Mn<sup>2+</sup>) doped hexagonal prismatic zinc oxide (ZnO) nanostructures for chemiresistive NO<sub>2</sub> sensor. *Sensors Actuators B Chem.* **380**, 133293 (2023). <https://doi.org/10.1016/j.snb.2023.133293>

Springer Nature or its licensor (e.g. a society or other partner) holds exclusive rights to this article under a publishing agreement with the author(s) or other rightsholder(s); author self-archiving of the accepted manuscript version of this article is solely governed by the terms of such publishing agreement and applicable law.